

## Foil-thickness dependence of projectile $K$ -satellite x-ray yields in the $L$ -shell nonequilibrium region

T. Mizogawa,\* Y. Awaya, T. Kambara, Y. Kanai, M. Kase, and H. Kumagai  
*The Institute of Physical and Chemical Research (RIKEN), Wako, Saitama 351-01, Japan*

P. H. Mokler

*Gesellschaft für Schwerionenforschung, 6100 Darmstadt, Federal Republic of Germany*

K. Shima

*Tandem Accelerator Center, University of Tsukuba, Tsukuba, Ibaraki 305, Japan*

(Received 14 March 1990)

We have studied projectile  $K$  x-ray satellite yields in collisions between 50-MeV  $\text{Ar}^{Q+}$  ions ( $Q=4, 6, 11, 12, 13$ ) and C foils with various thicknesses ( $2\text{--}100\ \mu\text{g}/\text{cm}^2$ ). For foil thicknesses below about  $10\ \mu\text{g}/\text{cm}^2$ ,  $Q$  dependence of the yields has been observed, reflecting the nonimmediate  $L$ -shell equilibrium. For this region, it has been shown that the mean  $K$ -hole formation cross section also varies with the target thickness and  $Q$ . The variation has been attributed to the varying chance of  $K$ -to- $L$  excitation with the increase or decrease of  $L$  holes in solid. The projectile charge fractions after passage through the target have also been measured for the foil-thickness region  $2\text{--}20\ \mu\text{g}/\text{cm}^2$  including the thicknesses for which charge-state equilibrium is not attained. By combining these data, the  $K$ -hole formation cross section specifying the number of  $L$  holes at the initial stage of a collision has been estimated. The results have been compared with theoretical predictions for cross sections of  $K$ -to-continuum ionization and  $K$ -to- $L$  excitation.

### I. INTRODUCTION

Dynamic processes of swift heavy ions colliding with solids have been widely investigated in these two decades.<sup>1-17</sup> A considerable part of these works has been performed by detecting emitted  $K$  x-rays from either projectiles or targets. In this case, it is well known that the  $K$  x-ray yields are not always proportional to the target thickness, and the reasons are considered as follows. First, the target-thickness dependence of the  $K$  x-ray yield reflects the multicollisional effects concerning  $K$ -shell processes.  $K$ -hole-bearing ions in solid may experience not only spontaneous decays, via Auger or x-ray emission processes, but also collisional quenchings, such as an electron capture. Thus the  $K$  x-ray yield does not have a simple relation with a  $K$ -hole formation cross section, even if the cross section is a well-defined constant. Second, the target-thickness dependence of  $K$  x-ray yield reflects nonimmediate outer-shell (especially  $L$ -shell) equilibrium. The quantities concerning  $K$ -shell processes, such as a  $K$ -hole formation cross section, actually depend on an outer-shell configuration of the ion. For example, a  $K$ -to- $L$  excitation cross section is directly affected by the number of  $L$  holes carried by the ion at the initial stage of a collision. Thus the  $K$ -hole formation cross section varies with the penetration depth through the development of  $L$ -shell holes.

If one applies suitable models or analyzing schemes to the analysis of the target-thickness dependence of  $K$  x-ray yield, some physical quantities concerning the dynamic processes of ions in solids can be estimated as described below.

Betz *et al.*<sup>1</sup> developed a model which treats the above-mentioned multicollisional effects concerning  $K$ -shell processes. In their model, the fraction of  $K$ -hole-bearing ions in solid varies with the penetration depth according to a rate equation containing several adjustable parameters (a  $K$ -hole formation cross section, a cross section of collisional quenching of  $K$  hole, and a  $K$ -hole lifetime). The parameters are assumed to be constant and are determined by fitting the solution of the rate equation to the experimental data of the x-ray yield. Similar procedures, called two- or three-component model, were applied by many groups.<sup>2-14</sup>

The models, however, do not take into account the above-mentioned effect of nonimmediate outer-shell equilibrium which is prominent for thin targets. Shima and co-workers<sup>15,16</sup> showed that the projectile  $K$  x-ray production cross section and the energy shifts drastically vary with the target thickness for the thin-target region where the development of  $L$  holes takes place. They attributed the observed thickness dependence to the influence of varying magnitudes of  $K$ -to- $L$  excitation cross section and the mean fluorescence yield with the penetration depth.

Rozet and Chetoui<sup>17</sup> presented a revised Betz model, where the influence of nonimmediate  $L$ -shell equilibrium on the  $K$  x-ray yield is taken into account. They showed that their model can extract a new information, e.g., an information about ionization of the  $2p\pi$  molecular orbital (MO), as well as the parameters dealt with in the Betz model. Their model may be appropriate only for near-symmetric collisions, for which MO processes are predominant to create  $K$  holes.

In a major part of the above-referred-to studies, they used semiconductor detectors [usually Si(Li) detectors] for x-ray detection. By using such detectors, one cannot resolve the satellite peaks of  $K\alpha$  or  $K\beta$  x-rays. Each of the satellites corresponds to a different outer-shell (especially  $L$ -shell) configuration, which results in a different fluorescence yield and a different lifetime. For the thin-target region, this complicates the thickness dependence of  $K$  x-ray yields and violates the validity of the above-mentioned two- or three-component model. By resolving such a satellite peak, however, we can obtain the more detailed information on the development of  $K$ -,  $L$ -, and  $M$ -shell configurations of ions in solid. Thus the utilization of a crystal spectrometer in foil-thickness-dependence experiments is desirable to study the effects of nonimmediate outer-shell equilibrium on  $K$ -hole development in solid.

Several works on target-thickness dependence using a crystal spectrometer were performed.<sup>2-4,13</sup> They studied, however, the collisions in the relatively thick-target region, where the equilibrium of an  $L$  shell has already been attained. In this thickness region, existing two- or three-component model can be applied to the analysis.

New experimental and analyzing procedures will be necessary for further investigation of the effects of nonimmediate  $L$ -shell equilibrium, especially for asymmetric systems. We report here the measurements of the yields of projectile  $K$  x-ray satellites in collisions between 50-MeV  $\text{Ar}^{Q+}$  ions ( $Q=4, 6, 11, 12,$  and  $13$ ) and a C-foil target with various thicknesses ( $2\text{--}100\ \mu\text{g}/\text{cm}^2$ ) using a broad-range crystal x-ray spectrometer.<sup>18</sup> A preliminary result has already been reported elsewhere.<sup>19</sup> The present collision system is far from symmetric, and the MO process is not important.

Our main purpose is a quantitative assessment of the role of  $K$ -to- $L$  excitation cross sections of ions in solid, which is influenced by nonimmediate  $L$ -shell equilibrium. To analyze the obtained data, we do not adopt a version of the parameter-fitting approach based on rate equations. A more straightforward method is adopted by utilizing well-established literature values of relevant quantities and reasonable assumptions. Furthermore, the charge-state distribution of the 50-MeV Ar ions after passage through C foils ( $2\text{--}20\ \mu\text{g}/\text{cm}^2$ ) and the projectile  $K$ -satellite yield for different impact energies (42 and 33.5 MeV) using a relatively thick target ( $20\ \mu\text{g}/\text{cm}^2$ ) have been also measured. The results are utilized for analyzing the data of the above-mentioned x-ray thickness-dependence measurements at 50 MeV.

## II. EXPERIMENT

### A. X-ray measurements

The present experimental setup is shown in Fig. 1. Fifty-MeV Ar ions from the accelerator known as RILAC (RIKEN linear accelerator), of which the charge state and the energy are analyzed by an analyzing magnet, are focused on a C-foil target to about a 1-mm-diam spot. The target is placed at the center of a vacuum chamber of which the diameter is 1 m. Typical pressure in the chamber is  $1 \times 10^{-6}$  Torr.

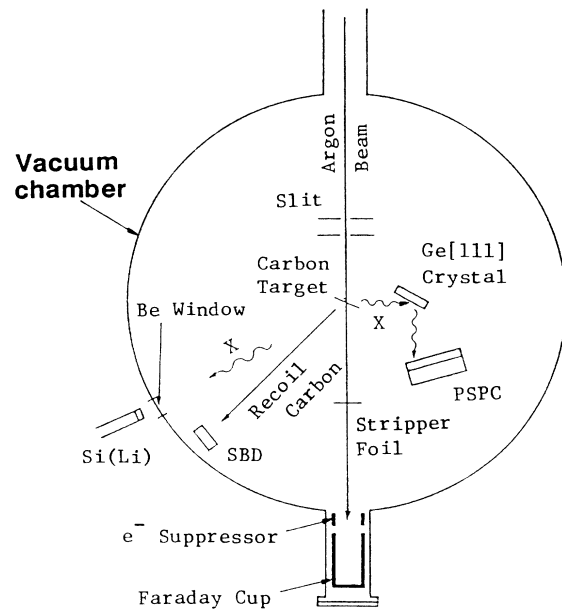


FIG. 1. Experimental setup for the target-thickness-dependence measurements of  $K$ -satellite yields.

Spectra of Ar  $K$  x rays emitted at the targets are measured by a broad-range crystal spectrometer,<sup>18</sup> consisting of a flat crystal and a position-sensitive proportional counter (PSPC). A flat Ge(111) crystal ( $24 \times 54\ \text{mm}^2$ ) is placed at the direction of  $90^\circ$  to the beam axis, with a Bragg angle  $2\theta=71^\circ$  for the center of the crystal. The distance from the target to the crystal is 15 cm, and the one from the crystal to the PSPC is 14 cm. The window of the PSPC is  $1 \times 10\ \text{cm}^2$  with 300- or 500- $\mu\text{m}$ -thick Be. In the present measurements, the spectrometer covers an energy range containing all the  $K\alpha$  satellites and most part of the  $K\beta$  satellites at once. Energy scale is determined by detecting He-ion induced Ag- $L$ , K- $K$ , and Cl- $K$  x rays from Ag and KCl targets under the same experimental geometry.

The lifetime of an essential part of  $K$ -hole bearing states is estimated to be shorter than  $10^{-13}$  sec [an order of magnitude of a theoretical value for a  $(1s)(2p)$  configuration<sup>20</sup>], and their decay occurs most at a distance of a few microns from the target. Metastable states which have much longer lifetimes are neglected in this paper.

The target carbon-foil thickness ranges from  $\sim 2$  to  $\sim 100\ \mu\text{g}/\text{cm}^2$  for  $\text{Ar}^{4+}$  ions, and from  $\sim 2$  to  $\sim 20\ \mu\text{g}/\text{cm}^2$  for  $\text{Ar}^{6+}$ ,  $\text{Ar}^{12+}$ , and  $\text{Ar}^{13+}$  ions. For  $\text{Ar}^{11+}$  ions, only one ( $2.6\text{-}\mu\text{g}/\text{cm}^2$ ) target is used.

The beam after passage through the target passes a post stripper ( $20\text{-}\mu\text{g}/\text{cm}^2$  C foil) (see Fig. 1) to guarantee the charge equilibration of the beam entering a Faraday cup. Possible secondary electrons are repelled by a -1-kV biased electron suppressor in front of the Faraday cup. From the integrated current and the well-established data of the equilibrium mean charge,<sup>21</sup> the total number of incident ions is determined for each run. A surface-barrier detector (SBD), located at  $45^\circ$  to the beam direction,

monitors the number of recoil C to determine the target thickness multiplied by the incoming ion number according to the formula of Rutherford-scattering recoil cross section. Thus the target thickness itself can be determined for each run.

A Si(Li) detector is placed outside the vacuum chamber at  $60^\circ$  to the beam direction. The window of the vacuum chamber is made of  $50\text{-}\mu\text{m}$ -thick Be, and the distance between the Si(Li) and the window is 1 cm. This detector is used to evaluate the absolute scale of the x-ray production cross sections for each  $K$  satellite observed by the crystal spectrometer, and to monitor the possible impurities in the target or the serious change in beam profile near the target.

Typical spectrum obtained by the crystal spectrometer is shown in Fig. 2, where  $KL^n$  denotes a satellite line originated from an initial state having  $n$   $L$  holes and one  $K$  hole. Yield of each satellite line is determined by a least-squares fitting method.

Absolute experimental satellite x-ray production cross sections are determined separately, as follows. The correction factor due to reflectivity of the crystal is calculated for each satellite according to the "mosaic model."<sup>22</sup> The correction factor for the absorption by the Be window and the counter gas of the PSPC is also calculated for each satellite by using absorption coefficients in the

literature.<sup>23</sup> These are done in a relative manner so that the correction factors for the  $KL^5$  satellite are equal to 1. The yield of each satellite line is multiplied by these relative correction factors. The sum of the corrected  $K$ -satellite yields is normalized to the absolute  $K$  x-ray production cross section measured by using the Si(Li) and SBD detectors. Thus the obtained "overall efficiency" of the crystal spectrometer is used to determine the individual satellite x-ray production cross section absolutely.

During the irradiation of ion beam on C foil, we have observed the increase of the foil thickness due to the deposition of C in the residual gas. Therefore a run is terminated when the increase of the thickness exceeds  $0.5\ \mu\text{g}/\text{cm}^2$ , for thin targets. The spectra obtained by several foils of which thicknesses are approximately equal (within  $\pm 0.25\ \mu\text{g}/\text{cm}^2$  difference) are added up to get the better statistics.

Impurities in the foil, which can be monitored by the elastic-recoil detection using the SBD, are mainly a few tenth of  $\mu\text{g}/\text{cm}^2$  H, N, and O. Disturbance by them is not serious, because the roles of N and O are similar to C, and the Ar  $K$ -hole formation cross section by H impact is small. Amounts of heavier elements are little, for scattered Ar ions observed by the SBD are very few, and there is little indication of impurities in the spectrum obtained by the Si(Li).

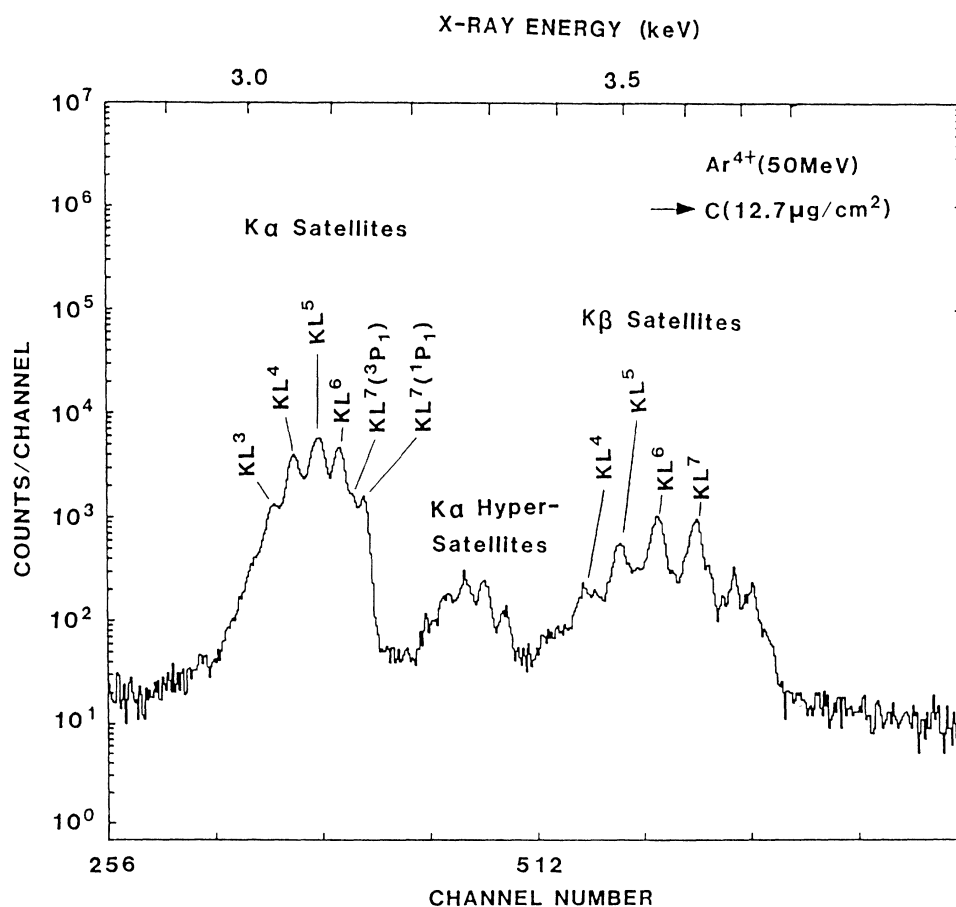


FIG. 2. Typical spectrum of Ar  $K$  x rays obtained by the broad-range crystal spectrometer.

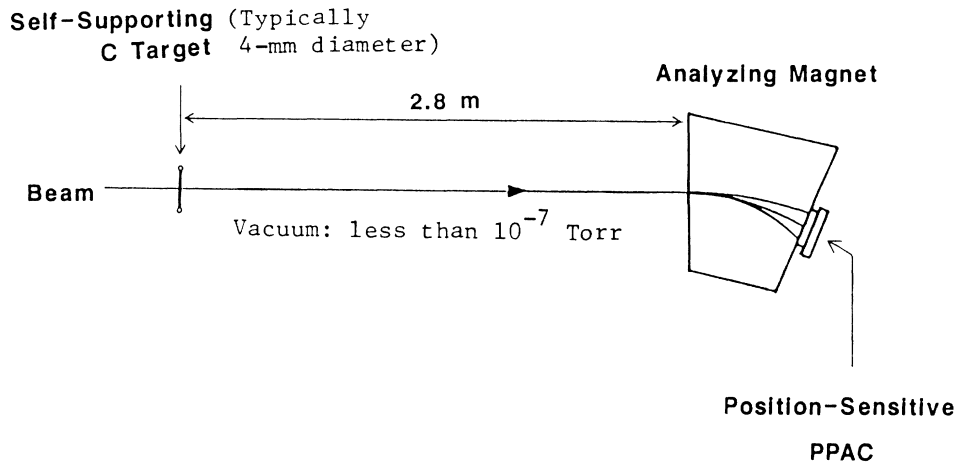


FIG. 3. Experimental setup for the measurements of charge-state distributions.

### B. Charge-state distribution measurements

The charge-state distributions of 50-MeV Ar ions after passage through thin C foils have also been measured as a function of C-foil thickness. Incident charge states are  $4+$  and  $12+$ , and the ranges of thickness are  $2\text{--}20$  and  $2\text{--}10 \mu\text{g}/\text{cm}^2$  for incident  $\text{Ar}^{4+}$  and  $\text{Ar}^{12+}$ , respectively. The experimental arrangement is shown in Fig. 3. The charge states after the passage through a foil are analyzed by a sector magnet and a position-sensitive parallel-plate

avalanche counter (PPAC). The specification of the magnet and the PPAC are given elsewhere.<sup>24</sup> Typical charge spectrum is shown in Fig. 4. The charge states  $4+$  to  $16+$  are covered by six measurements with six different field strengths. Any two measurements with adjacent field strengths cover at least one common charge state, for the purpose of normalization. Throughout the charge-state distribution measurement, no visible change in target profile is observed.

## III. RESULTS AND DISCUSSION

### A. Results for $K\alpha$ satellites

The experimental  $K\alpha L^n$  x-ray production cross section, i.e., the yield of the satellite per incident ion divided by target atomic thickness (atoms per unit area), is denoted as  $\bar{\sigma}_x(n)$ . The results of  $\bar{\sigma}_x(n)$  for the incidences  $\text{Ar}^{4+}$  and  $\text{Ar}^{12+}$  are shown in Figs. 5 and 6, respectively, as a function of the target thickness.

The results for the projectile  $\text{Ar}^{6+}$  show essentially the same feature of target-thickness dependence as for  $\text{Ar}^{4+}$ . That is, the magnitude of  $\bar{\sigma}_x(n)$  for  $n \geq 5$  tends to increase with the thickness up to near  $10 \mu\text{g}/\text{cm}^2$  and decrease slowly above  $\sim 20 \mu\text{g}/\text{cm}^2$ , and  $\bar{\sigma}_x(n)$  for  $n \leq 3$  decreases rapidly up to near  $5 \mu\text{g}/\text{cm}^2$  and remains approximately constant above there. The value of  $\bar{\sigma}_x(4)$  shows slow decrease with an increase to the target thickness.

The results for the projectile  $\text{Ar}^{13+}$  are similar to those for  $\text{Ar}^{12+}$ , but the values  $\bar{\sigma}_x(n)$  of the former are generally higher than those of the latter, especially for high  $n$ . In both sets of the data, the values monotonously decrease with increasing the thickness.

Incident-charge dependence of  $\bar{\sigma}_x(n)$  appears to diminish at around  $20 \mu\text{g}/\text{cm}^2$  within the experimental error as shown in Figs. 5 and 6. As shown in Fig. 5 for  $\text{Ar}^{4+}$ , the  $\bar{\sigma}_x(n)$  for any  $n$  in this region tends to decrease slowly with increasing target thickness. This can be interpreted partly as the multicollisional effect which has been treated with the two- or three-component model<sup>1-14</sup> and partly as the effect of energy loss of ions in solid.

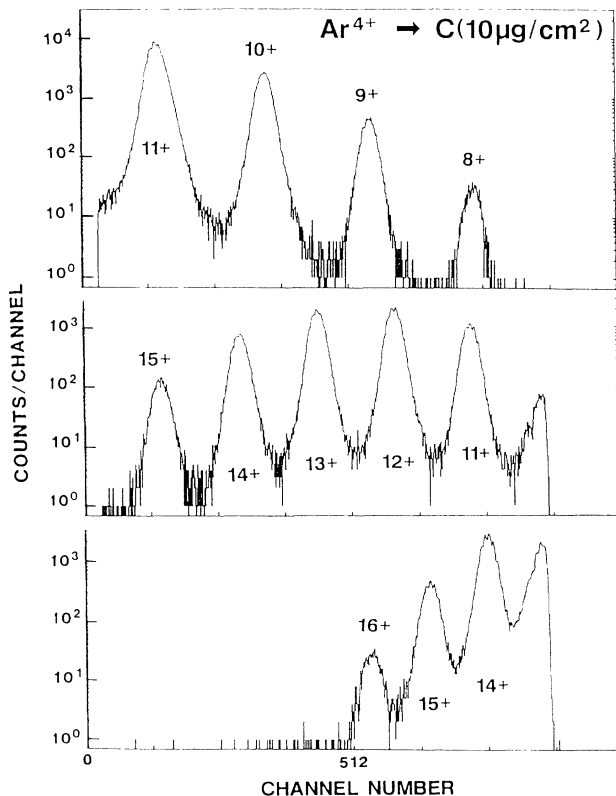


FIG. 4. Typical charge spectrum.

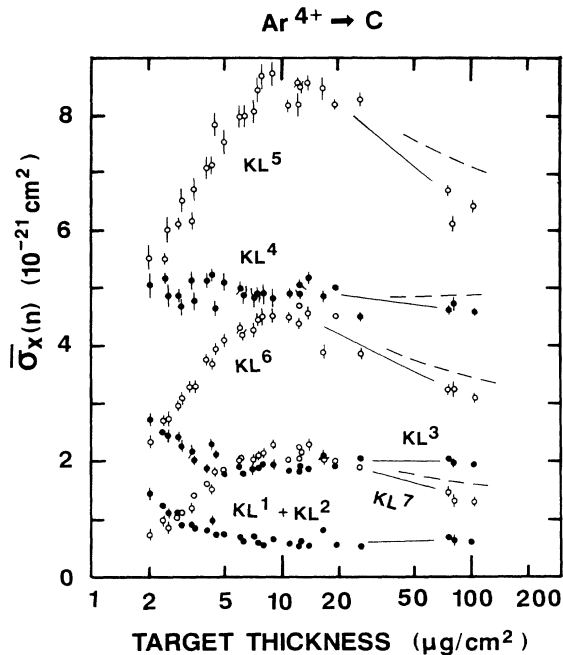


FIG. 5. Mean Ar  $K\alpha$  x-ray satellite cross section as a function of C-foil thickness. The projectile is 50-MeV  $\text{Ar}^{4+}$ . Solid lines are drawn only to guide the eye. Dashed lines are the curves after correction for the effect of yield decrease due to the projectile energy loss in the target (see text.).

To estimate the overall effects of energy loss, we have performed a subsidiary measurement of the energy dependence of  $\bar{\sigma}_x(n)$  using a  $20\text{-}\mu\text{g}/\text{cm}^2$ -thick C target and 33.5, 42, and 50 MeV Ar ions. The results are shown in Fig. 7. At this thickness, we can neglect the influence of the  $L$ -shell nonequilibrium in the first-order approxi-

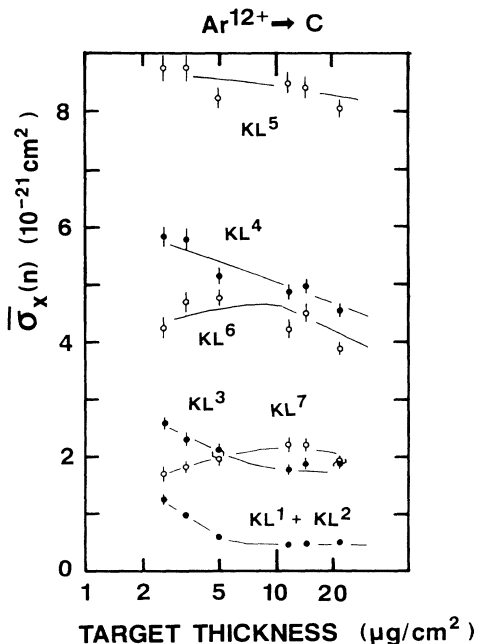


FIG. 6. Same as Fig. 5, except that the projectile is  $\text{Ar}^{12+}$ .

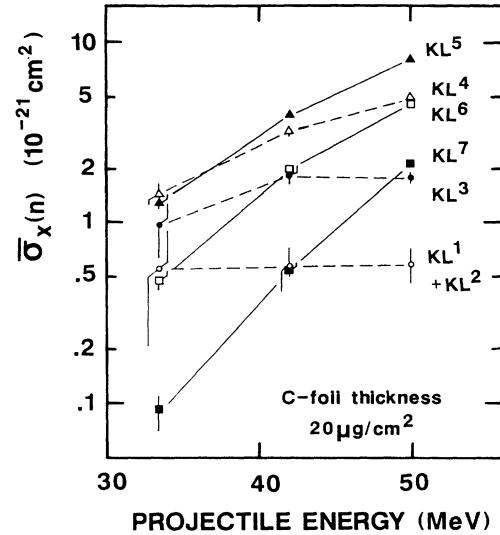


FIG. 7. Energy dependence of mean Ar  $K$  x-ray satellite cross sections.

mation. Therefore, using the obtained energy dependence, we can correct the  $\bar{\sigma}_x(n)$  for thick ( $\geq 20\text{ }\mu\text{g}/\text{cm}^2$ ) targets in the thickness-dependence measurements to estimate the  $\bar{\sigma}_x(n)$  which will be expected when the energy loss does not take place. The results of such a “correction” are shown in Fig. 5 by dashed curves. The remaining decreasing feature of  $\bar{\sigma}_x(n)$  versus the target thickness can be attributed to the effect of collisional quenching of  $K$  holes, which has been dealt with by the usual two- or three-component model. In the present paper, we do not discuss more about this region. We focus on the thinner-target region, where the effect of nonimmediate  $L$ -shell equilibrium has a vital importance.

#### B. Results for $K\beta/K\alpha$ ratios: $M$ -electron number in solid

The observed trend of target-thickness dependence for  $K\beta$  satellites is very similar to that for  $K\alpha$ . Figure 8 shows the target-thickness dependence of  $K\beta L^n/K\alpha L^n$  ratios for the projectile  $\text{Ar}^{4+}$ . The ratios remain approximately constant with the change of target thickness. This is a remarkable observation, for the usual (total  $K\beta$ )/(total  $K\alpha$ ) ratio obtained by using a Si(Li) detector varies with the target thickness in this thickness region. Such a total ratio is usually regarded as a measure of a ratio of  $M$ -shell electron population and  $L$ -shell population and is considered to vary with the  $L$ - and  $M$ -shell population. In the present case, however, we are considering the  $K\beta/K\alpha$  ratio with specifying the initial  $L$ -hole number  $n$ . Therefore the ratio is a measure of  $M$ -shell electron population only. The above-mentioned observation is an evidence for the immediate equilibration of the  $M$  shell.

From these  $K\beta L^n/K\alpha L^n$  ratios, we can estimate the number of  $M$  electrons at the moment of the  $K$  x-ray emission by comparing them with theoretical values specifying  $L$ - and  $M$ -shell configurations. Figure 9 displays the experimental  $K\beta L^n/K\alpha L^n$  ratios for  $n \geq 4$

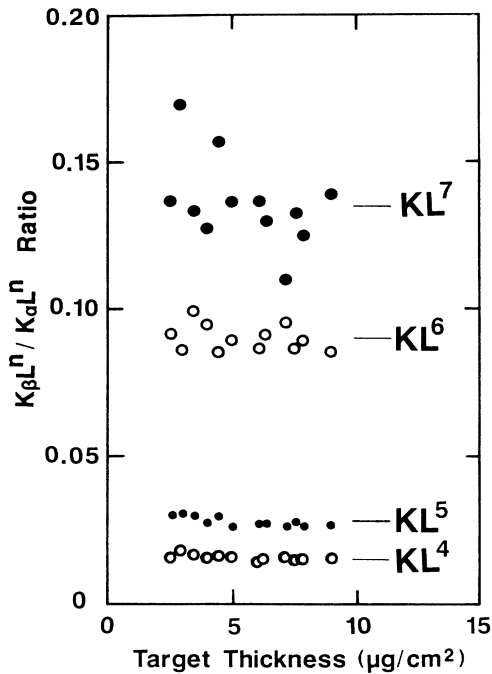


FIG. 8.  $K\beta L^n / K\alpha L^n$  ratios as a function of the target thickness for  $\text{Ar}^{4+}$ -C collisions.

together with theoretical curves calculated by using Bhalla's<sup>20</sup> transition rates. Here, for different initial  $L$ -shell configurations with the same  $L$ -hole number, the transition rates are averaged assuming that the electrons are randomly distributed over the  $2s$  and  $2p$  orbitals. We can see that the experimental ratios are several times below the theoretical curve for the case where only one

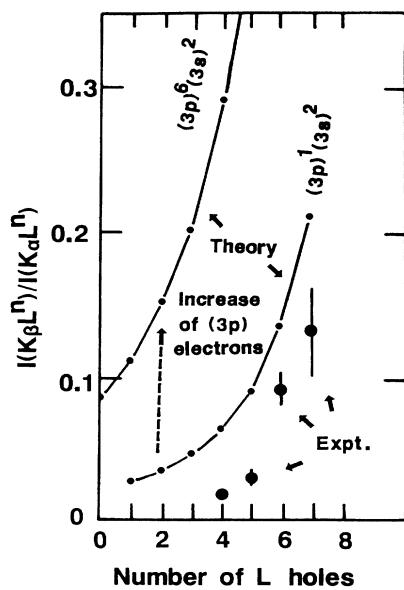


FIG. 9. Comparison between theoretical  $K\beta/K\alpha$  ratios specifying  $L$ - and  $M$ -shell configurations and the experimental data of  $K\beta L^n / K\alpha L^n$  shown in Fig. 8.

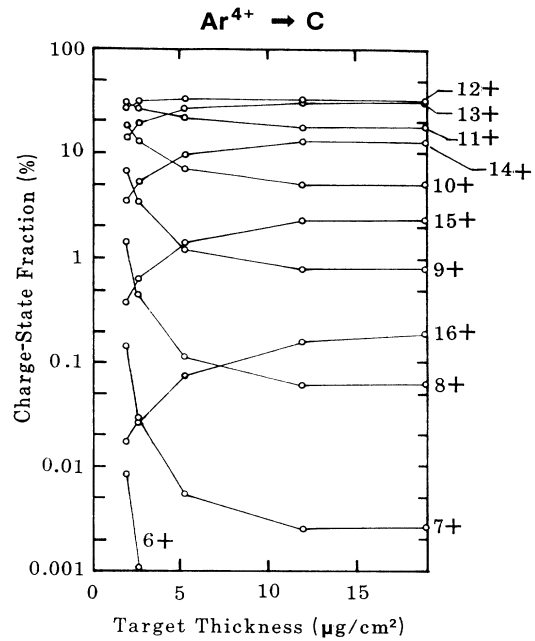


FIG. 10. The charge-state distributions of Ar ions as a function of the C-foil target thickness.  $\text{Ar}^{4+}$  is the incident ion.

$3p$  electron exists.

From these data, we conclude that the average number of  $M$  electrons is much less than unity. By considering the immediate equilibration of  $M$  shell, this conclusion may be valid for Ar ions traversing the target without carrying  $K$  holes.

C. Results for charge-state distribution measurements

The results of charge-state distribution of 50-MeV Ar ions are given in Figs. 10 and 11 for the incident charge-

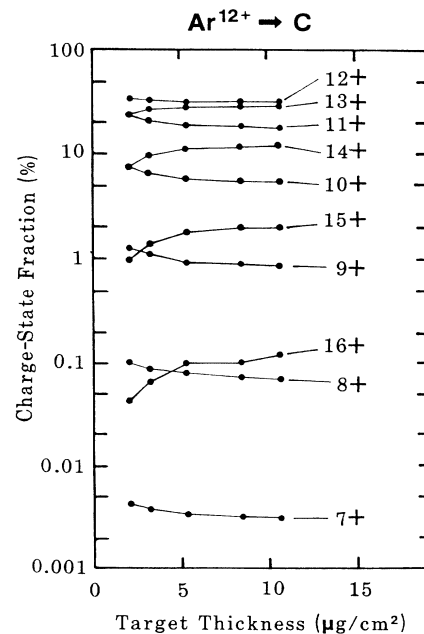


FIG. 11. Same as Fig. 10, except that the incident ion is  $\text{Ar}^{12+}$ .

states 4+ and 12+, respectively, as a function of the target thickness. The figures suggest that the charge-state distribution reaches its equilibrium around  $10 \mu\text{g}/\text{cm}^2$ . The nonimmediate  $L$ -shell equilibrium below about  $10 \mu\text{g}/\text{cm}^2$  affects the cross section of  $K$ -hole formation and causes the thickness and projectile charge dependence of the  $K$ -satellite yields shown in Figs. 5 and 6, which will be discussed later.

#### D. $K$ -hole formation

In this section, we adopt a reasonable assumption that the fraction of  $K$ -hole-bearing ions in solid is small compared with unity, and the fraction of double  $K$ -hole-bearing ions is negligibly small. Validity of this will be quantitatively discussed later.

To extract the information about  $K$ -hole formation from the present data of  $\bar{\sigma}_x(n)$ , we first consider the following equation exhibiting the balance of total  $K$ -hole formation events and total  $K$ -hole filling events,

$$\bar{\sigma}_v = \bar{\sigma}_a + \bar{\sigma}_c, \quad (1)$$

where  $\bar{\sigma}_v$  is the effective  $K$ -hole formation cross section, i.e., the total  $K$ -hole formation events per ion divided by the target atomic thickness (atoms per unit area),  $\bar{\sigma}_a$  is the mean spontaneous  $K$ -hole decay cross section, i.e., the total number of Auger and radiative  $K$ -hole decay per ion divided by the target atomic thickness, and  $\bar{\sigma}_c$  is the mean cross section for the collisional  $K$ -hole quenching, i.e., the total number of collisional  $K$ -hole quenching per ion divided by the target atomic thickness. The  $\bar{\sigma}_v$  is defined by

$$\bar{\sigma}_v = \frac{1}{d} \int_0^d \sum_n \sigma_v(n) Y_{0n}(x) dx, \quad (2)$$

where  $d$  is the target atomic thickness,  $\sigma_v(n)$  is the  $K$ -hole formation cross section for the ions having  $n$   $L$  holes and no  $K$  hole at the initial stage of a collision, and  $Y_{0n}(x)$  is the fraction of ions having  $n$   $L$  holes and no  $K$  hole at the depth  $x$ . The  $\bar{\sigma}_a$  is the quantity that can be deduced from the experimental  $\bar{\sigma}_x(n)$  as follows.

$$\bar{\sigma}_a = \frac{\bar{\sigma}_x(n)}{\omega_n}, \quad (3)$$

where  $\omega_n$  is the mean fluorescence yield for each  $K\alpha L^n$  satellite. The  $\bar{\sigma}_c$  is defined by

$$\bar{\sigma}_c = \frac{1}{d} \int_0^d \sigma_c Y_1(x) dx, \quad (4)$$

where  $\sigma_c$  is the collisional  $K$ -hole quenching cross section, and  $Y_1(x)$  is the fraction of  $K$ -hole-bearing ions at the depth  $x$ .

Considering that  $\sigma_c Y_1(x)$  approaches to zero for small  $x$ , its average over  $x$ ,  $\bar{\sigma}_c$ , also approaches to zero for small  $d$ . Therefore we obtain an approximation for  $\bar{\sigma}_v$ :

$$\bar{\sigma}_a \xrightarrow{d \rightarrow 0} \bar{\sigma}_v. \quad (5)$$

It will be also noteworthy that the zero-thickness limit of  $\bar{\sigma}_v$  becomes equal to  $\sigma_v(n_0)$  according to Eq. (2),

where  $n_0$  is the number of  $L$  holes carried by incident ions before entering the target. The goal of this section is to evaluate the  $\sigma_v(n_0)$ , which can be directly compared with theoretical predictions. This will be performed through the analysis of  $\bar{\sigma}_a$  using a simple model and the charge-state distribution data.

Figure 12 shows the value  $\bar{\sigma}_a$  obtained from  $\bar{\sigma}_x(n)$  values and Eq. (3) as a function of the target thickness. Here the mean fluorescence yields  $\omega_n$  are calculated using Bhalla's transition rates,<sup>20</sup> by the same manner as the calculation of  $K\beta L^n/K\alpha L^n$  in Sec. III B. For relatively thick targets, the incident-charge dependence of  $\bar{\sigma}_a$  is not seen; meanwhile, gradually decreasing behavior of  $\bar{\sigma}_a$  is observed with the increase of the target thickness. This is due to the effects of the projectile energy loss and the collisional quenching, as mentioned previously. The approximate behavior of  $\bar{\sigma}_a$  "corrected" for energy-loss effect is also shown in Fig. 12 by a dashed curve.

On the other hand, in the region  $d \lesssim 10 \mu\text{g}/\text{cm}^2$ , the value  $\bar{\sigma}_a$  drastically varies with the target thickness and the incident charge state. For the projectiles  $\text{Ar}^{4+}$  and  $\text{Ar}^{6+}$ , it increases, and, for the projectiles  $\text{Ar}^{12+}$  and  $\text{Ar}^{13+}$ , it decreases with the increase of the target thickness. This incident charge-state dependence of  $\bar{\sigma}_a$  may be more impressive when  $\bar{\sigma}_a$  for extremely thin targets ( $\sim 2.6 \mu\text{g}/\text{cm}^2$ ) is plotted against the incident charge state of Ar ions (Fig. 13). It can be seen that the values for  $\text{Ar}^{4+}$  and  $\text{Ar}^{6+}$  are approximately same, whereas those for  $\text{Ar}^{11+}$ ,  $\text{Ar}^{12+}$ , and  $\text{Ar}^{13+}$  show roughly linear-increasing behavior with increasing charge. The bend is located at around 8+, which corresponds to the state of

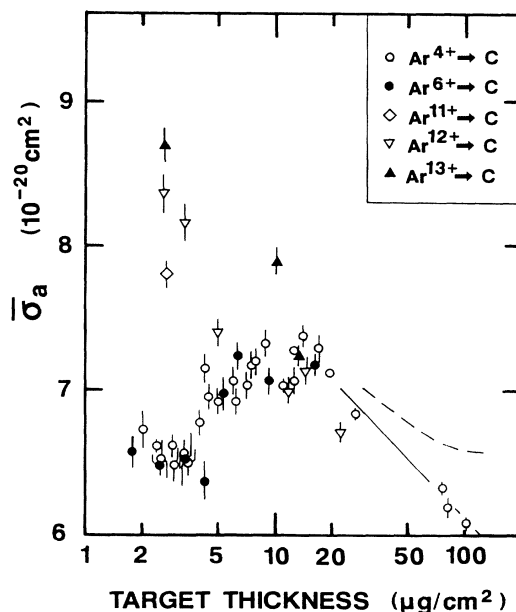


FIG. 12. "Mean spontaneous  $K$ -hole decay cross section"  $\bar{\sigma}_a$  as a function of C-foil thickness (see text). Open circle,  $\text{Ar}^{4+}$ ; solid circle,  $\text{Ar}^{6+}$ ; diamond,  $\text{Ar}^{11+}$ ; open triangle,  $\text{Ar}^{12+}$ ; solid triangle,  $\text{Ar}^{13+}$ . A solid line is to guide the eye. A dashed line shows the curve after correction for the effect of yield decrease due to the projectile energy loss in the target (see text).

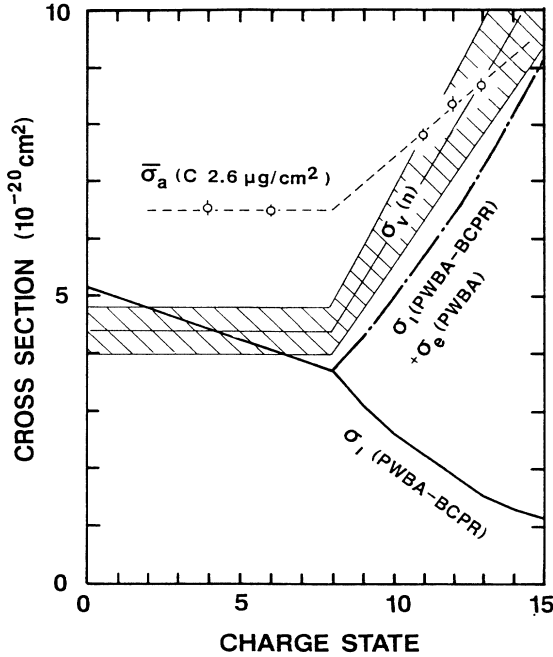


FIG. 13. Comparison among experimental and theoretical cross sections for  $K$ -hole formation specifying initial  $L$ -hole number. Open circle, experimental “mean spontaneous  $K$ -hole decay cross section” for thin targets (see text). A thin dashed line is drawn to guide the eye. A thin solid line indicates the experimental  $K$ -hole formation cross section based on a model described in the text. Vertical width of hatched area indicates the statistical error. The thick solid line indicates the theoretical cross sections of  $K$ -shell ionization based on PWBA-BCPR (see text). Dot-dashed line is the sum of the theoretical cross sections for the  $K$ -shell ionization (PWBA-BCPR) and the  $K$ -to- $L$  excitation (PWBA).

Ar ions with a fully occupied  $L$  shell.

This observation clearly indicates that the  $\sigma_v(n)$  in Eq. (2), the  $K$ -hole formation cross section specifying the  $L$ -hole number at the initial stage of a collision, really depends on  $n$ , because the zero-thickness limit of  $\bar{\sigma}_a$  gives  $\sigma_v(n)$  as mentioned before.

A quantitative evaluation of this zero-thickness limit is considered in the following. We assume the presence of the following simple relation:

$$\sigma_v(n) = \sigma_I + nS_e, \quad (6)$$

where  $\sigma_I$  is a part of  $\sigma_v(n)$  independent on the initial  $L$ -hole number  $n$ , and the second term is another part of  $\sigma_v(n)$  which increases with  $n$ . The  $S_e$  is a constant. The  $\sigma_I$  can be interpreted as a  $K$ -to-continuum ionization cross section for the ions having no  $L$  hole at the initial stage of a collision. For the ions initially having some  $L$  holes, however, the ionization cross section will decrease with increasing  $n$  because of the increase of  $K$ -shell binding energy. The second term includes such an  $n$  dependence, as well as the contribution of  $K$ -to- $L$  excitation cross section.

After averaging over the penetration depth  $x$  and the  $L$ -hole number  $n$ , we get the relation

$$\bar{\sigma}_v = \sigma_I + \bar{n}_L S_e, \quad (7a)$$

$$\bar{n}_L = \frac{1}{d} \int_0^d n_L(x) dx, \quad (7b)$$

$$n_L(x) = \sum_n n Y_{0n}(x), \quad (7c)$$

where  $n_L(x)$  is the mean number of  $L$  holes carried by the ions having no  $K$  hole at the depth  $x$ . If the value  $n_L$  is known from the charge-state distribution data, the values  $\sigma_I$  and  $S_e$  can be deduced from the experimental data of  $\bar{\sigma}_a$  in the region where the target thickness is thin enough to neglect the contribution of the collisional quenching of a  $K$  hole. The mean number of  $L$  holes is obtained by

$$n_L(x) = q(x) - n_M^{(eq)}, \quad (8)$$

where  $n_M^{(eq)}$  is the number of  $M$  holes in equilibrium, under the assumption that the  $M$  shell reaches its equilibrium at the depth smaller than the thickness of the thinnest target used in the present measurements, and  $q(x)$  is the mean charge for the given depth  $x$ . From the  $K\beta/K\alpha$  ratio we have found that the average  $M$ -electron number is much less than unity. Here we adopt the  $M$ -hole number with a rather conservative error limit, as follows.

$$n_M^{(eq)} = 7.4 \pm 0.4. \quad (9)$$

We have assumed that the value  $q(x)$  in solid is equal to the mean charge obtained in the charge-state distribution measurements for the target thickness  $x$ , because of the following reason. Since the residual  $M$ -electron number at the exit surface has been shown to be a few tenth of unity from the  $K\beta/K\alpha$  data (see Fig. 9), the effect of post-foil charge increase due to  $LMM$  Auger and  $LLM$  Coster-Kronig processes can be neglected. A predominant process of  $M$ -electron deexcitation is a radiative transition to an  $L$  hole (if exists), which does not cause charge increase.

In Fig. 14, values of  $n_L$  are plotted against  $x$ . Interpolating these data including the given zero-thickness value ( $n_L=0$  and 4 for  $\text{Ar}^{4+}$  and  $\text{Ar}^{12+}$ , respectively) by straight lines, integration of Eq. (7b) is performed. Thus, obtained  $\bar{n}_L$  values are also plotted in Fig. 14. The  $\sigma_I$  and  $S_e$  values can be evaluated as follows.

$$\bar{\sigma}_v[12+] = \sigma_I + S_e \bar{n}_L[12+], \quad (10a)$$

$$\bar{\sigma}_v[4+] = \sigma_I + S_e \bar{n}_L[4+], \quad (10b)$$

where  $\bar{\sigma}_v[Q+]$  and  $\bar{n}_L[Q+]$  indicate the  $\bar{\sigma}_v$  and  $\bar{n}_L$  values obtained for incident  $\text{Ar}^{Q+}$  ions. By solving these equations,

$$\sigma_I = \frac{\bar{n}_L[4+] \bar{\sigma}_v[12+] - \bar{n}_L[12+] \bar{\sigma}_v[4+]}{\bar{n}_L[4+] - \bar{n}_L[12+]}, \quad (11a)$$

$$S_e = \frac{\bar{\sigma}_v[4+] - \bar{\sigma}_v[12+]}{\bar{n}_L[4+] - \bar{n}_L[12+]}. \quad (11b)$$

We limit our discussion to an extremely thin target ( $\sim 2.6 \mu\text{g}/\text{cm}^2$ ). Then we obtain the following values for  $\sigma_I$  and  $S_e$ :

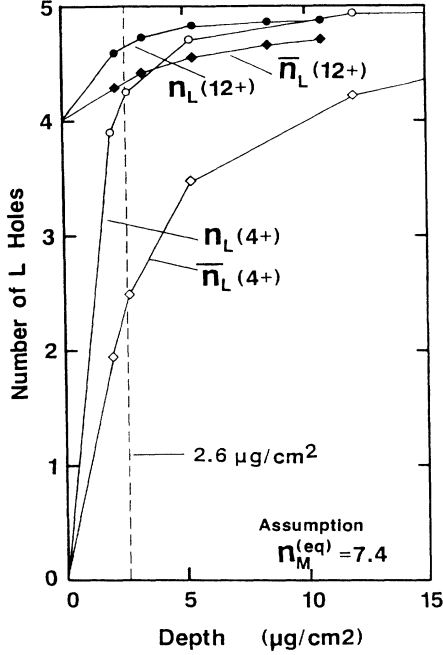


FIG. 14. Average Ar-ion  $L$ -hole number in the C-foil (see text).

$$\sigma_I = (4.4 \pm 0.4) \times 10^{-20} \text{ cm}^2, \quad (12a)$$

$$S_e = (0.87 \pm 0.09) \times 10^{-20} \text{ cm}^2. \quad (12b)$$

The uncertainty above contains only errors originated from statistical errors of raw spectrum data. Another error source is the uncertainty of  $n_M^{(eq)}$ , which causes  $\pm 8\%$  error. The error caused by the neglect of the collisional quenching of  $K$  hole is small for a thin target and tends to cancel in Eq. (11). We discuss this problem later.

Finally we obtain from Eqs. (6) and (12),

$$\sigma_v(n) = (4.4 + 0.87n) \times (1 \pm 0.1) \times 10^{-20} \text{ cm}^2. \quad (13)$$

This result is also shown in Fig. 13.

### E. Comparison to theory

Theoretical calculations for  $K$ -to-continuum ionization and  $K$ -to- $L$  excitation cross sections are made as follows. The present collision system is regarded as  $C^{6+}$  impact on Ar ion targets. The ionization cross section of an Ar ion specifying the initial  $L$ -hole number is calculated by the plain-wave Born approximation<sup>25</sup> with the corrections for "increased binding energy,"<sup>26,27</sup> "polarization,"<sup>27</sup> "Coulomb deflection,"<sup>26,27</sup> and "relativistic effect."<sup>28</sup> We refer to this approximation as PWBA-BCPR. In this calculation, the "outer-shell screening parameter"  $\Theta_K$ ,

$$\Theta_K = \frac{I_K}{Z_{2K}^2 I_H}, \quad (14)$$

where  $I_K$  is a  $K$ -shell ionization potential of the target (an Ar ion), is evaluated by using a theoretical  $I_K$ ,<sup>29</sup> because precise experimental values for highly ionized Ar ions are

not available. Here  $Z_{2K}$  is  $Z_2 - 0.3 = 17.7$ , and  $I_H$  is the hydrogen ionization potential (13.6 eV).

Among the corrections, the former two are found predominant and result the reduction by a factor  $2 \sim 4$  from the simple PWBA. The latter two contribute by only a few percent.

For the cross section of  $K$ -to- $L$  excitation, no available theory containing a correction scheme for the distortion-like "binding" and "polarization" effects seems to exist. Here we calculate it based on a simple PWBA. For the collisions of a bare nucleus, of which the atomic number is  $Z_1$ , and a hydrogenlike target, of which the atomic number is  $Z_2$ , a well-known scaling law<sup>30</sup> is available.

$$\sigma_i(v, Z_1, Z_2) = \frac{Z_1^2}{Z_2^4} \sigma_i \left( \frac{v}{Z_2}, 1, 1 \right), \quad (15)$$

where  $v$  is the projectile velocity,  $i$  indicates the relevant excitation channel, and  $\sigma_i(v, 1, 1)$  is the cross section for proton-hydrogen collisions.<sup>30</sup> We replace  $Z_2$  with  $Z_{2K} = Z_2 - 0.3$  and multiply by 2 ( $K$ -electron number) for heliumlike targets. To obtain the total  $K$ -to- $L$  excitation cross section for the targets having  $n$  initial  $L$  holes, the cross sections for  $1s$ - $2s$  and  $1s$ - $2p$  excitations are summed and multiplied by  $n/8$ .

$$\sigma_e(n) = 2 \left[ \frac{n}{8} \right] \left[ \frac{Z_1^2}{Z_{2K}^4} \right] \left[ \sigma_{1s-2s} \left( \frac{v}{Z_{2K}}, 1, 1 \right) + \sigma_{1s-2p} \left( \frac{v}{Z_{2K}}, 1, 1 \right) \right]. \quad (16)$$

Thus calculated theoretical results are also shown in Fig. 13.

The PWBA-BCPR for ionization cross sections are known to agree with experimental results within a discrepancy of a few tens of percent for the collisions similar to the present (e.g., 4–38-MeV  $B$ -ion bombardment on targets K, Ca, etc.<sup>31</sup>). Such an agreement is found again in Fig. 13, for the Ar ion charge state below  $8+$  (no  $L$  hole). For the charge state above  $8+$ , there can be also seen remarkable agreement between the experimental  $\sigma_v(n)$  and the sum of the theoretical cross sections. The theoretical  $K$ -to- $L$  excitation cross section is, however, based on a simple PWBA, and the distortion effect is not taken into account. There are two possible interpretations. First, both the present theoretical cross sections may be trustworthy. In this case, we can conclude that the distortion effect is not important for the  $K$ -to- $L$  excitation. Second, both the theoretical cross sections may contain significant errors which tend to cancel each other. In this case, the above agreement is fortuitous, and the further refinement of theories for ionization and excitation of highly ionized targets is necessary. The present experimental and analysis procedure offers a good tool for testing their validity.

### F. Collisional quenching of $K$ hole

In the above discussion, we have neglected the influence of the collisional quenching of  $K$  hole. Here, we show that this is roughly justified by estimating the col-

lisional quenching cross section from the experimental data. First, for the incidences of  $\text{Ar}^{12+}$ —or  $\text{Ar}^{13+}$ , the  $\bar{\sigma}_v$  values are almost independent on the penetration depth, because the  $L$ -hole number at the entrance of solid is nearly equal to that of the equilibrated beam [see Eq. (7)]. Therefore the left-hand side of Eq. (1) is approximately constant for these projectiles. The first term of the right-hand side in Eq. (1) has been evaluated experimentally. Thus the second term, i.e., the contribution of the collisional quenching, can be estimated by a subtraction of  $\bar{\sigma}_a$  from  $\bar{\sigma}_v$ , although the energy-loss effect should be corrected for the thick targets as described before.

Furthermore, according to the well-known two-component model,<sup>1</sup> we can easily show that

$$\bar{\sigma}_c \xrightarrow{d \rightarrow 0} \frac{1}{2} \sigma_c \bar{\sigma}_v d . \quad (17)$$

Thus the quenching cross section itself can be deduced from the slope of  $\bar{\sigma}_a$  near the zero thickness. The uncertainty depends on how accurately the slope can be read from the data.

In the present measurement, only the estimate of the order of magnitude can be possible. We conclude  $\sigma_c = (5 \pm 3) \times 10^{-19} \text{ cm}^2$  from the data shown in Fig. 12. Thus the contribution of the second term in Eq. (1) for the extremely thin targets ( $\sim 2.6 \mu\text{g}/\text{cm}^2$ ) is less than 10%, of which the influence on the above-evaluated  $\sigma_v(n)$  is a few percent.

#### G. Fraction of $K$ -hole-bearing ions, $Y_1(x)$

In above discussion we have consistently assumed  $Y_1(x) \ll 1$ . Validity of this can be shown as follows. The fraction of ions which experiences a  $K$ -hole formation in solid is  $\approx \bar{\sigma}_v d$ . For the  $10\text{-}\mu\text{g}/\text{cm}^2$  target, this is only 5% of total projectiles at most. A considerable part of this may experience the  $K$  hole filling in solid. Thus the  $Y_1(x)$  never exceeds 5%.

#### IV. SUMMARY AND CONCLUDING REMARKS

We have performed the measurements of the target thickness and projectile charge dependence of projectile  $K$ -satellite yields for 50-MeV Ar ions and C-foil targets,

with a crystal x-ray spectrometer. The influence of nonimmediate  $L$ -shell equilibrium has been clearly observed in the resulted mean  $K$ -satellite x-ray production cross sections. With the aid of theoretical fluorescence yields specifying the number of  $L$  holes at  $K$ -hole decay, it has been shown that the mean  $K$ -hole formation cross section itself varies with the target thickness and the charge state of incident ions. This has been attributed to the varying contribution of the  $K$ -to- $L$  excitation cross section. By combining the results of charge-state distribution measurements with those of the above x-ray measurements, and adopting a simple model, the  $K$ -hole formation cross sections specifying the  $L$ -hole number at the initial stage of a collision have been evaluated for zero target-thickness limit. The results are in good agreement with the sum of a theoretical  $K$ -to-continuum ionization cross section (PWBA-BCPR) and a theoretical  $K$ -to- $L$  excitation cross section (PWBA). The necessity of further refinement of theoretical approximation has been pointed out.

In the present analysis, several approximations and/or assumptions have been adopted, but their validity and the ambiguity of the results can be easily assessed from the experimental data. This is one of the merits of a procedure without parameter fitting.

This is the first work in which a crystal x-ray spectrometer is adopted to investigate the influence of nonimmediate  $L$ -shell equilibrium on  $K$ -hole formation in solid. The experimental technique and the analyzing scheme outlined above have been successfully applied to the present collision system,  $\text{Ar}^{Q+}$  on C at 1.25 MeV/amu. We have suffered, however, from the instability of the thin targets. We suggest that more high- $Z$  projectiles with higher incident energy will yield further fruitful results by application of the present technique, because of the higher  $L$ -shell equilibration thickness.

#### ACKNOWLEDGMENTS

We wish to acknowledge the operational and technical group of the Linac Laboratory of the Institute of Physical and Chemical Research (RIKEN) for their valuable help. We would like to thank M. Nishida for her assistance with the data handling.

\*Present address: Nagaoka National College of Technology, Nagaoka, Niigata 940, Japan.

<sup>1</sup>H. D. Betz, F. Bell, H. Panke, G. Kalkoffen, M. Welz, and D. Evers, *Phys. Rev. Lett.* **33**, 807 (1974).

<sup>2</sup>H. Panke, F. Bell, H. D. Betz, W. Stehling, E. Spindler, and R. Laubert, *Phys. Lett.* **53A**, 457 (1975).

<sup>3</sup>F. Bell, H. D. Betz, H. Panke, W. Stehling, and E. Spindler, *J. Phys.* **B 9**, 3017 (1976).

<sup>4</sup>H. Panke, F. Bell, H. D. Betz, and W. Stehling, *Nucl. Instrum. Methods* **132**, 25 (1976).

<sup>5</sup>K. O. Groeneveld, B. Kolb, J. Schader, and K. D. Sevier, *Z. Phys.* **A 277**, 13 (1976).

<sup>6</sup>T. J. Gray, P. Richard, K. A. Jamison, and J. M. Hall, *Phys. Rev. A* **14**, 1333 (1976).

<sup>7</sup>T. J. Gray, C. L. Cocke, and R. K. Gardner, *Phys. Rev. A* **16**, 1907 (1977).

<sup>8</sup>C. L. Cocke, S. L. Varghese, and B. Curnutte, *Phys. Rev. A* **15**, 874 (1977).

<sup>9</sup>R. K. Gardner, T. J. Gray, P. Richard, A. Schmiedekamp, K. A. Jamison, and J. M. Hall, *Phys. Rev. A* **15**, 2202 (1977).

<sup>10</sup>A. Schmiedekamp, T. J. Gray, B. L. Doyle, and U. Schiebel, *Phys. Rev. A* **19**, 2167 (1979).

<sup>11</sup>J. A. Tanis, W. W. Jacobs, and S. M. Shafroth, *Phys. Rev. A* **22**, 483 (1980).

<sup>12</sup>J. A. Tanis, S. M. Shafroth, J. E. Willis, and J. R. Mowat, *Phys. Rev. Lett.* **45**, 1547 (1980).

<sup>13</sup>R. L. Watson, A. Langenberg, R. A. Kenefick, C. C. Bahr, and J. R. White, *Phys. Rev. A* **23**, 2471 (1981).

- <sup>14</sup>K. D. Sevier, Gy. Szabo, and F. Folkmann, *J. Phys. B* **14**, 4065 (1981).
- <sup>15</sup>K. Shima, K. Umetani, T. Mikumo, H. Kano, Y. Tagishi, M. Yamanouchi, H. Yamaguchi, and Y. Iguchi, *Phys. Lett.* **77A**, 427 (1980).
- <sup>16</sup>K. Shima, K. Umetani, and T. Mikumo, *Nucl. Instrum. Methods* **194**, 353 (1982).
- <sup>17</sup>J. P. Rozet and A. Chetioui, *J. Phys. B* **14**, 73 (1981).
- <sup>18</sup>A. Hitachi, H. Kumagai, and Y. Awaya, *Nucl. Instrum. Methods* **195**, 631 (1982).
- <sup>19</sup>T. Mizogawa, Y. Awaya, T. Kambara, Y. Kanai, M. Kase, H. Kumagai, P. H. Mokler, and K. Shima, *Nucl. Instrum. Methods Phys. Res. A* **262**, 141 (1987).
- <sup>20</sup>C. P. Bhalla, *Phys. Rev. A* **8**, 2877 (1973).
- <sup>21</sup>K. Shima, T. Mikumo, and H. Tawara, *At. Data Nucl. Data Tables* **34**, 357 (1986); A. B. Wittkower and H. D. Betz, *At. Data* **5**, 113 (1973).
- <sup>22</sup>A. Burek, *Space Sci. Instrum.* **2**, 53 (1976).
- <sup>23</sup>E. Storm and H. I. Israel, *Nucl. Data Tables A7*, 565 (1970).
- <sup>24</sup>Y. Kanai, Y. Awaya, T. Kambara, M. Kase, H. Kumagai, T. Mizogawa, and K. Shima, *Nucl. Instrum. Methods Phys. Res. A* **262**, 128 (1987).
- <sup>25</sup>G. S. Khandelwal, B. H. Choi, and E. Merzbacher, *At. Data* **1**, 103 (1969).
- <sup>26</sup>G. Basbas, W. Brandt, and R. Laubert, *Phys. Rev. A* **7**, 983 (1973).
- <sup>27</sup>G. Basbas, W. Brandt, and R. Laubert, *Phys. Rev. A* **17**, 1655 (1978).
- <sup>28</sup>J. S. Hansen, *Phys. Rev. A* **8**, 822 (1973).
- <sup>29</sup>R. J. Maurer and R. L. Watson, *At. Data Nucl. Data Tables* **34**, 185 (1986).
- <sup>30</sup>D. R. Bates and G. Griffing, *Proc. Phys. Soc., London, Sect. A* **66**, 961 (1953).
- <sup>31</sup>G. Monigold, F. D. McDaniel, J. L. Duggan, R. Rice, A. Totten, R. Mehta, and P. D. Miller, *Phys. Rev. A* **18**, 380 (1978).